Nanobiotechnol (2009) 5:34–41
DOI 10.1007/s12030-009-9030-8

Biosynthesis of Stable Polyshaped Gold Nanoparticles from Microwave-Exposed Aqueous Extracellular Anti-malignant Guava (*Psidium guajava*) Leaf Extract

D. Raghunandan · S. Basavaraja · B. Mahesh · S. Balaji · S. Y. Manjunath · A. Venkataraman

Published online: 6 October 2009

Abstract Addition of microwave-exposed aqueous extracellular anti-malignant guava (*Psidium guajava*) leaf extract to the aqueous gold chloride solution yielded stable polyshaped gold nanoparticles of high composition. Microwave-assisted route selected for the preparation of aqueous guava leaf extract was to suppress the enzymatic action. The formation of nanoparticles was understood from the UV–visible and X-ray diffraction studies. The size and shape analysis was done using field emission scanning electron microscopy, transmission electron microscopy, and atomic force microscopy. Zeta potential experiment shows that the bio-functionalized gold nanoparticles colloidal solution obtained as above will maintain its stability even after 30 weeks of storage. It is observed that the flavonoids which are separated during microwave heating of extracellular solution of the guava leaves are responsible for the biosynthesis of gold nanoparticles.

B. Mahesh · S. Balaji · A. Venkataraman (✉)
Materials Chemistry Laboratory, Department of Material Science,
Gulbarga University,
Gulbarga 585106, Karnataka, India
e-mail: raman_chem@rediffmail.com

D. Raghunandan
H.K.E.S's College of Pharmacy,
Sedam Road,
Gulbarga 05, Karnataka, India

S. Basavaraja
Veeco-India Nanotechnology Laboratory,
Jawaharalal Nehru Cetre for Advanced Scientific Research,
Bangalore 64, India

S. Y. Manjunath
Sri Krupa, Institute of Pharmaceutical Science,
Village Velkatta, Siddipeth,
Medak, AP, India

Keywords microwave · guava (*Psidium guajava*) leaf extract · polyshaped · gold nanoparticles · zeta potential

Introduction

The optoelectronic and physicochemical properties of nanoscale materials are size and shape dependent. Polyshaped nanoparticles, which resemble certain bacteria, can more easily infiltrate human cells, and this suggests that using the polyshape of nanoparticles can make them more effective in treating diseases [1]. The general medical applications of nanoparticles have been reviewed by Salata [2].

Gold, especially in nanosize, is widely used in emerging interdisciplinary field of nanobiotechnology [3, 4]. Their displayed novel properties have more effective and wider biomedical applications [5–11]. These properties of polyshaped gold nanoparticles (AuNP) have different behaviors and make them suitable for therapeutic utilization. Biological molecules and neoplastic cells can be readily attached to the surface of AuNP, and the plasmon resonances of such bioadsorbed AuNP of certain shapes cause them to have greater photon capture cross-sections than those of photo thermal dyes [12]. Bio-detection sensitivity of AuNP is often associated with their physical and chemical properties depending on the shape [13, 14]. AuNP with different dimensions have been widely applied to detect biological molecules [15]. Colloidal AuNP are used to detect specific DNA sequences and single-base mutations in a homogeneous format [16].

The nanoparticle synthesis techniques fall under two categories: "bottom–up" and "top–down" approaches. With the development of top–down chemical and physical methods, the concern for environmental contaminations is heightened as the chemical procedures involved in the

synthesis of nanomaterials generate a large amount of hazardous byproducts. Among the various synthesis routes, bio-based "bottom–up" protocol promises a better chance to obtain nanostructures of more homogeneous chemical composition and with fewer defects [17]. With the voracious demand for biosynthesized nanoparticles, this recently developed field offers many new routes. These include employing microorganisms, such as: *Fusarium oxysporum* [18], *Fusarium semitactum* [19, 20], *Cladosporium* sp. [21], and also different plants like alfalfa [22] and neem [23]. Biosynthesis of metal nanoparticles from different microorganisms is a well-known concept, but use of plants is gaining much importance because of its nonpathogenicity and offers low or nil toxic profiles. Possibility of using this process can be thought of on a large scale. Our research is focused on the microwave-exposed aqueous extracellular guava leaf extract for gold nanoparticle synthesis.

The rate of synthesis of AuNP from microwave-exposed guava leaf extract is compared to those of chemical and physical methods, and it is noted that this has an excellent time-related advantage over benign and conventional method of metal nanoparticle synthesis from microorganisms and other plants [22, 23]. Unlike microbial nanoparticle synthesis, the current method holds an advantage of being simple, carried out at ambient temperature, and synthesized with a high level of reproducibility. The stability of these gold nanoparticle suspensions stored for 30 weeks was analyzed using zeta potential instrument. The study infers that the stability of colloidal AuNP synthesized using aqueous guava leaf extract is more than that of nanoparticles synthesized from microorganisms [18–21].

Recently, Sastry et al. synthesized Au, Ag, and Au–Ag bimetallic Au core–Ag shell nanoparticles using neem (*Azadicachta indica*) leaf broth has consumed 2–4 h of time for the process [23]. The current method of AuNP synthesis from guava leaf extract offers a great time-related advantage as the entire process is completed within few minutes (90% of the reduction of Au^{3+} ions to AuNP takes place within 5 min).

Twenty-five different reported anti-malignant plants were screened including the popular anti-malignant Vinca (*Vinca rosea*) plant. Guava (*Psidium guajava*) leaf, which is also known for its anti-malignant effects, was selected after confirming its potentiality for further preparation of extract, synthesis of AuNP, and for screening. The extracellular guava leaf extract which contained a variety of flavonoids is commonly used in subtropical countries as a dietary supplement because of its various pharmacological effects like antioxidant and anti-malignant activities [24–27]. In fact, it was reported that the fermented guava leaf extract suppressed lipopolysaccharide-induced macrophage cancer cells [28]. However, only limited studies demonstrated that the plants were used to synthesize the AuNP with a preview of having synergic anti-malignant activity.

Materials and Methods

Preparation of the Reaction Solutions

Carefully weighed 10^{-3} M $HAuCl_4$ aqueous solution was used for the synthesis of AuNP. For preparing the aqueous extracellular solution of guava leaves (*P. guajava*) for biosynthesis, 10 g of freshly collected guava leaves cut into appropriate size (~ 5 cm×1 cm) was taken in a 250-ml wide-neck Borosil conical flask and washed several times with deionized water. Deionized water (200 ml) was added to the flask containing washed, freshly cut guava leaves and exposed to microwave for 3 min (DAEWOO, 2.45 GHz). The resultant crude extract was filtered with Whatman filter paper no. 40. Exactly 5 ml of the filtrate was then added to 50 ml of aqueous 10^{-3} M $HAuCl_4$ solution in a 250-ml Borosil flask and kept on a shaker at 27°C for the biosynthesis of AuNP.

Analysis

Periodically, aliquots of the reaction solution were removed and subjected to UV–vis spectroscopy measurements. The UV–vis spectroscopy measurements were performed on an ECIL 5704SS UV–visible spectrophotometer at a resolution of 1 nm. For the crystallinity studies, films of AuNP formed on Si (1 1 1) substrates by drop coating the colloidal nanoparticles were used for X-ray diffraction (XRD) study. The data were obtained using Siemens X-ray diffractometer (Japan), operated at 30 kV and 20 mA current with Cu $K\alpha$ (l=1.54 Å) radiation.

The morphology of the AuNP was examined using field emission scanning electron microscopy (FESEM, FEI Nova

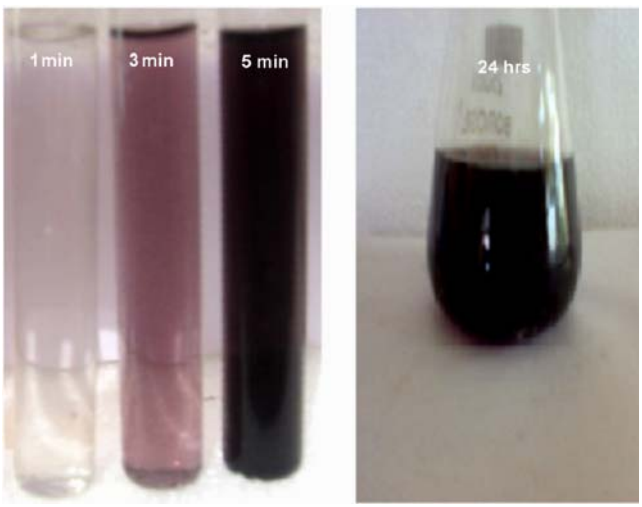

Fig. 1 Color intensity of AuNP. The intensity of color of the solution containing aqueous 10^{-3} M $HAuCl_4$ treated with microwave-exposed guava (*P. guajava*) leaf extract increases steadily as a function of reaction time.

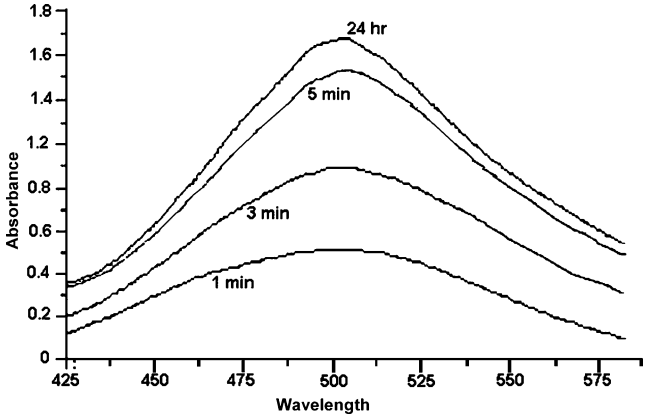

Fig. 2 UV–Visible spectra recorded as a function of time (λ_{max}=505 for AuNP). For brevity, data corresponding to all spectra are not plotted.

nano 600, Netherlands), and for this the images were operated at 15 kV on a 0° tilt position. The transmission electron microscopy (TEM) image of the sample was obtained using Technai-20 Philips transmission electron microscope operated at 190 keV. Atomic force microscopy (AFM) images were collected under ambient conditions on a Veeco Innova scanning probe microscope. Etched Si nanoprobe tips (RTESPA-M) were used for the same. AuNP powder sample was prepared by centrifuging the synthesized AuNP solution at 10,000 rpm for 15 min for Fourier transformed infrared radiation (FTIR) Spectroscopy measurements. The solid residue layer which contains AuNP was redispersed in sterile deionized water three times to remove the unattached biological impurities. The pure residue was then dried perfectly in an oven overnight at 65°C. The thus obtained powder was subjected to FTIR measurements carried out on a Perkin-Elmer Spectrum-One instrument at a resolution of 4 cm^{-1} in KBr pellets.

Zeta potential of the AuNP colloidal solution stored up to 30 weeks in ambient conditions was sonicated and measured using a PALS Zeta Potential Analyzer ver. 3.54 (NCL, Pune).

Results and Discussion

In this paper, we stress on the use of microwave-exposed aqueous extracellular guava leaf extract for the synthesis of gold nanoparticles (AuNP) from aqueous $HAuCl_4$ solution. (i.e., through the reduction of Au^{3+} to Au^0). The initial color of the solution after the addition of microwave-exposed aqueous guava leaf solution to aqueous $HAuCl_4$ solution was colorless. The intensity of the color of reaction mixture changes to dark purple with in 5 min. This shows that the reaction medium behaves with time kinetics; the same is shown in Fig. 1. The color developed in the solution as a result of the formation of AuNP. The same is observed with a surface plasmon resonance (SPR) peak in the UV–visible spectroscopy. This important observation indicates that the reduction of the Au^{3+} ions takes place extracellularly. Color of the AuNP found to be dark purple in water is due to excitation of the SPR in metal nanoparticles [29]. The biosynthesis reaction accelerates with the time, and the intensity of color of the reaction mixture increases rapidly. The process of biosynthesis is carried out at ambient environmental conditions, and the total reaction is completed within few minutes. It is observed that the surface plasmon peak occurs at 505 nm; the wavelength peak is shown in Fig. 2. The broadening and slight shifting of the SPR is probably due to the dampening of the surface plasmon resonance caused by the change in the refractive index of the surrounding medium and also due to the modification of the size and shape of the AuNP in colloidal solution. The reduction of the metal ions occurs very rapidly, and more than 90% of the reduction of Au^{3+} ions will be completed within 5 min. This is the fastest method of biosynthesis in comparison to the earlier

Fig. 3 XRD pattern of AuNP.

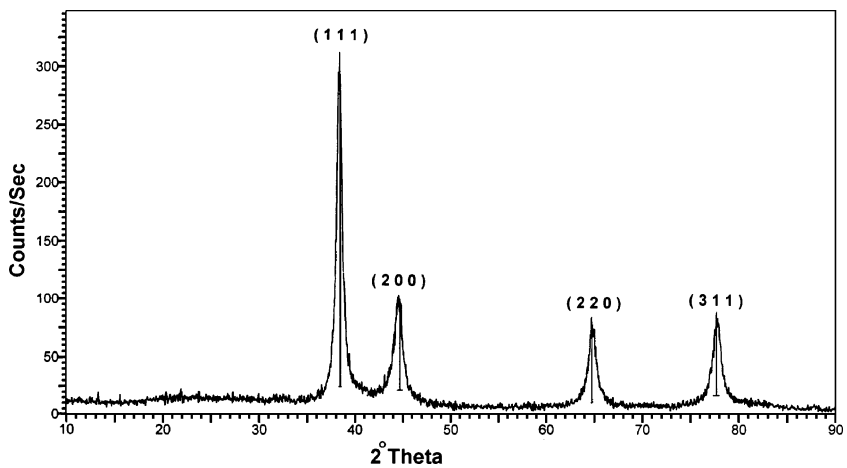

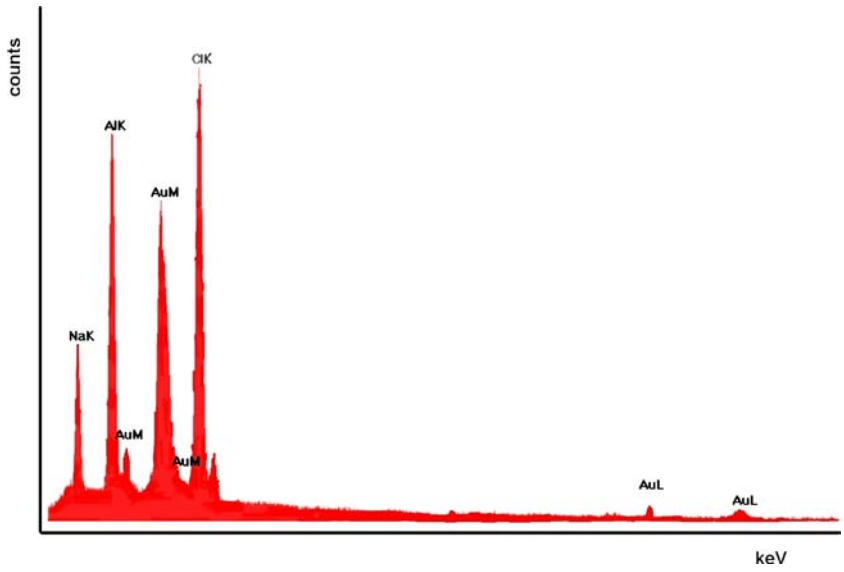

Fig. 4 EDAX graph of metallic AuNP.

conventional studies with other microorganism- [18–21] and plant-mediated [22, 23] synthesis. The time required for the conventional synthesis of AuNP from other plants was 2 to 4 h and from different microorganisms was 24 to 120 h and thus are rather slow.

Figure 3 shows the XRD pattern suggesting the crystalline nature of the AuNP synthesized from microwave-exposed aqueous extracellular guava leaf extract. The intense diffraction peaks due to AuNP are clearly observed at (111), (200) (220), and (311). These agree well with the reported standards JCPDS file no. 04-0784. This study infers the crystallinity of the AuNP obtained during biosynthesis. The mean particle diameter of AuNP was calculated from the XRD pattern according to the line width of the (1 1 1) refraction peak using the following Scherrer's equation:

$$D = \frac{K\lambda}{\beta_{1/2}\cos\theta}$$

The equation uses the reference peak width at angle θ, where α is the X-ray wavelength (1.5418 Å), $\beta_{1/2}$ is the width of the XRD peak at half height, and K is a shape factor which is 0.9 for spherical particles. The calculated average particle size of the Au was found to be 27 nm, which was also in line with the observation of the TEM results discussed later. The slight deviation of the band from 15^0 to 25^0 seen was due to organic moiety [19]. The energy-dispersive X-ray analysis study (EDAX) verifies the crystallinity of the particles AuNP, shown in Fig. 4.

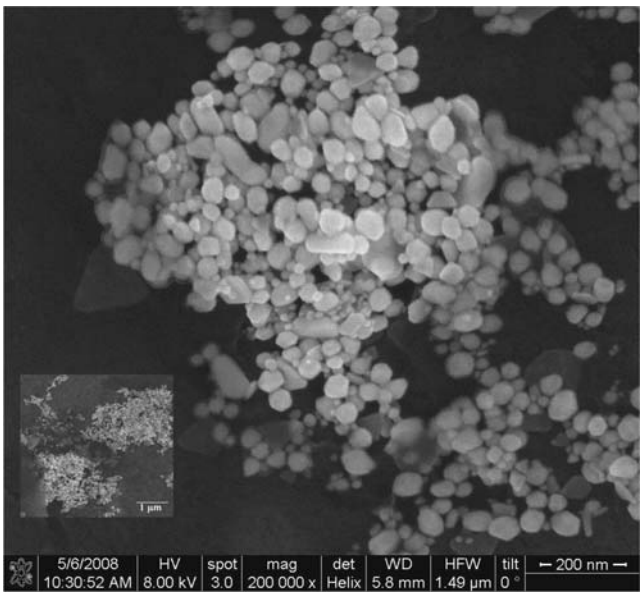

Fig. 5 FESEM images of AuNP. The *inset* shows the homogeneity of AuNP showed at 1 µm scale.

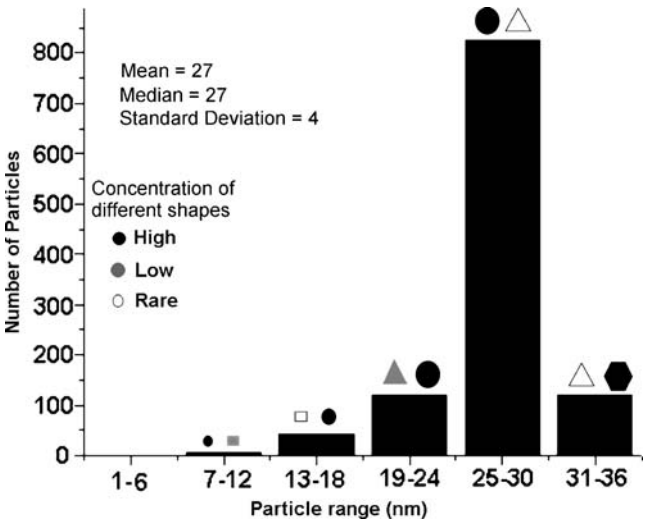

Fig. 6 Particle size distribution histogram of AuNP using FESEM measurements.

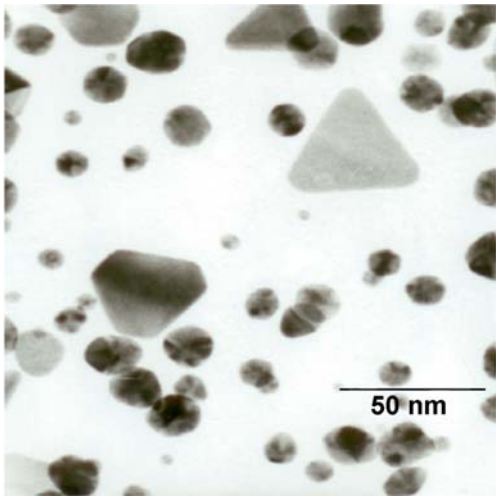

Fig. 7 TEM images of AuNP.

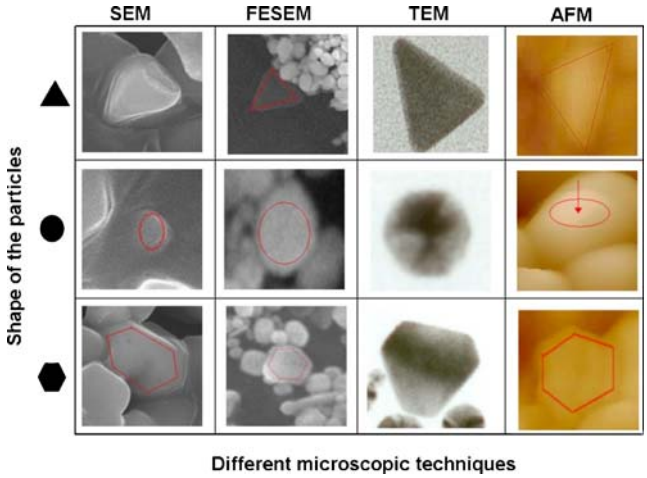

Fig. 9 Shapes of AuNP observed under different microscopic techniques.

Figure 5 shows the FESEM of synthesized AuNP on nanometric scale. The nanoparticles were uniformly distributed and are found to have formed in an aggregated state. On careful observation, AuNP are found to be surrounded by a thin layer of bio-moieties (mostly flavonoids) which seem to be responsible for reducing Au^{3+} ions to AuNP. Most of the particles are spherical in shape and monodispersed in nature with diameters in the range of 27±3 nm. The triangular and hexagonal shaped nanoparticles comparatively are in bigger size and probably have contributed for size variation. The same is reconfirmed with drop-coated TEM grids. It can be understood that the absolute monodispersity can be made possible by varying the other environments like pH of the extract, concentration of the aqueous salt solution, temperature, etc. of the reaction. The studies are under way.

The size and shape distribution histogram obtained for 1,107 nanoparticles is shown in Fig. 6. This histogram is prepared from the statistical data provided along with FESEM images. From this figure, it is observed that above 75% of the particles are in 24–29 nm range, and there is a marginal variation in the particle size. In this range, 95% of the particles are in spherical shape, and the remaining are of triangular shape. In this range, very rare pentagonal structures are also observed. In the 30–35 nm range, hexagonal nanoparticles are in high concentration, and the remaining are in triangular shape. Surprisingly, in this range, no spherical shaped nanoparticles are observed. At the lower range from 18 to 23 nm, triangular nanoparticles are also present in moderate concentration (~10%), and the remaining portion is of spherical nanoparticles only. Rod-shaped particles are seen in the lower range of 7–12 nm, but overall contribution of these shapes to the total number of nanoparticles taken for analysis is negligible (0.2%).

Figure 7 shows the typical bright-field TEM image of the biosynthesized AuNP. TEM technique was employed to visualize the size and shape of the AuNP formed. The TEM

Fig. 8 AFM images of AuNP.

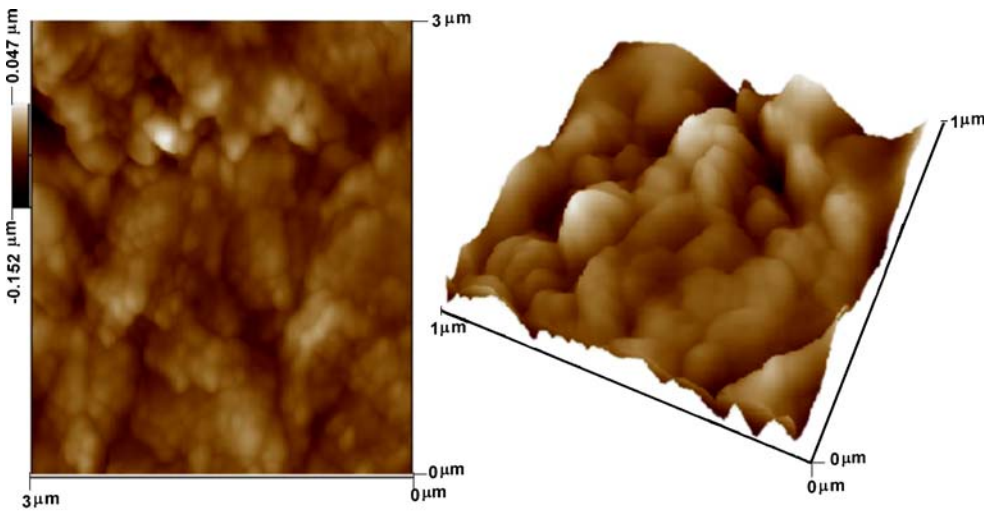

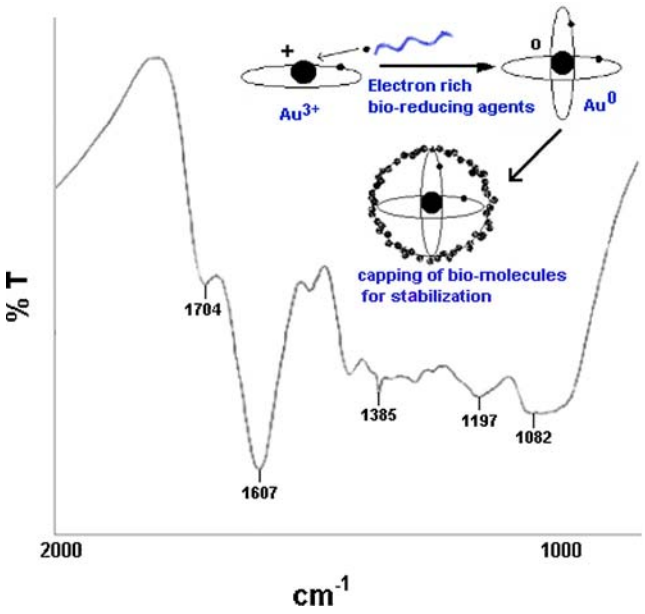

Fig. 10 FTIR spectra of dried, ultracentrifuged, and separated AuNP powder in KBR pellets. *Inset* shows the probable pathway of extracellular biosynthesis of AuNP from bioreducing agents of guava (*P. guajava*) leaf extract.

and FESEM images suggest that the particles are almost monodispersed and polyshaped. The TEM image infers that there are few triangular and hexagonal shaped particles, and the remaining are spherical shaped AuNP.

AFM is becoming an important biophysical technique for studying the morphology of nanoparticles and biomolecules [30]. The understanding of the functionalization of the AuNP synthesized from microwave-exposed aqueous extracellular extract of guava leaves is further confirmed by AFM measurements. The three-dimensional study of bio-functionalized AuNP is done by AFM and further compared with FESEM and TEM results. The AFM measurements were made using the tapping mode developed especially for studying bio-functionalized samples. Figure 8 shows typical, medium-scale AFM image (5 × 5 μm) of the bio-functionalized organic layer which consists of rich concentration organic moieties at the surface. From the topographical view, it is evident that most of the nanoparticles are in spherical and regular shapes. The root mean square value for roughness of the sample is only about 27 nm. The results as noted above in FESEM images of Fig. 4 and the TEM images of Fig. 5 are quite agreeable to the observations made under AFM results, and further studies are required to know the clear dimension of the thickness of the moieties covered on the nanoparticles. The particle size in the AFM images, ~40–60 nm, is

Fig. 11 Zeta potential studies of functionalized AuNP synthesized using aqueous guava extract with aqueous $AgNO_3$ solution after 30 weeks.

Measurement Parameters:

Zeta Potential Model	= Smoluchowski	Liquid	= Water
Mean Mobility	= -2.30 (μ/s) / (V/cm)	Temperature	= 25°c
pH	= 6.70	Viscosity	= 0.890 cP
Conductance	= 4.66 μs	Refractive Index	= 1.330
Concentration	= 2.00 mg/ml	Dielectric Constant	= 78.54

Instrumental Parameters:

Sample Count Rate	= 506 kcps	Voltage	= 4.00 volts
Ref. Count Rate	= 1172 kcps	Electric Field	= 7.07 V/cm
Wavelength	= 659.0 nm	Cycles Per Plan	= 10
Field Frequency	= 2.00 Hz		

Run	Zeta Potential (mV)
1	-30.25
2	-30.55
3	-30.30
4	-30.61
5	-30.51
Mean	-30.45
Std. Error	0.18

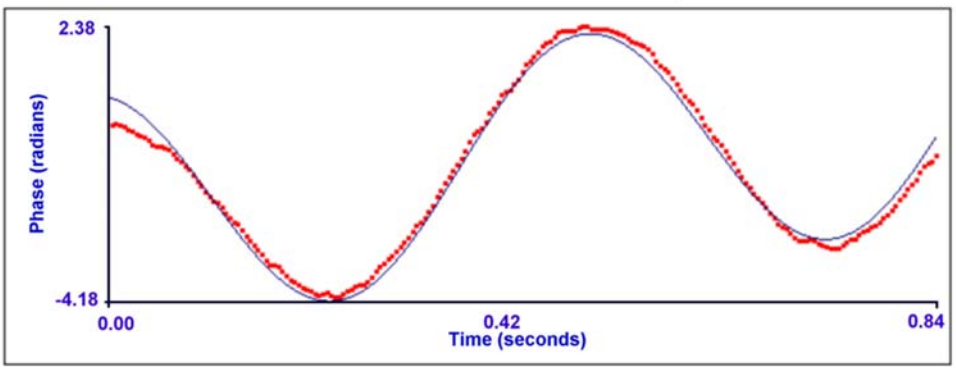

somewhat larger than the value determined from TEM measurements (~25–30 nm). This magnification is attributed to the convolution of true particle size with that of the AFM tip (increase in size and shape of AuNP observed in AFM may be influenced by the effect of tip-sample convolution). The individual polyshaped AuNP are clearly illustrated using different microscopic techniques in Fig. 9

The probable pathway of biosynthesis was studied using Fourier transformed infrared spectroscopy. Figure 10 shows that FTIR peaks at 1,704, 1,607, 1,385, 1,197, and 1,082 cm^{-1} represent the different functional groups of the adsorbed biomolecules on the surface of the AuNP. Absence of amide I and amide II peaks confirms the denaturing of proteins/enzymes in the guava extract after the microwave exposure. This also suggests the influence of other organic moieties in the synthesis and stabilization of AuNP. The probable pathway of bioreduction is shown as schematic diagram in inset of Fig. 10. We can presume that the flavonoids [31] and terpenoids [32], which are abundant in guava leaves, show characteristic absorption peaks that appear to be responsible for accelerated reduction and capping process. Terpenoids are poorly water soluble and hence may not be among prime moieties involved in the reduction process. The IR absorptions peaks (cm^{-1}) are noted as follows: 1,197 and 1,082 (–O–), 1,385 cm^{-1} (geminal methyl group, 1,607 (C=C, aromatic), 1,704 (α,β unsaturated ketone and esters). The peaks observed suggest the presence of flavonones adsorbed on the surface of the AuNP. It can be understood that the flavonoids could be adsorbed on the metal surface by interaction with carbonyl groups or π-electrons. The internal conversion mechanism of ketone group to carboxylic acid in flavonoids may influence the Au^{3+} ion reduction. The study is under way. The nanoparticles are almost of spherical shape and dispersed in nature with diameters in the range of 27± 3 nm. The same is reconfirmed with drop-coated TEM grids.

With the advent of nanobiotechnology, the study of colloids has become very important, especially in usage of these colloidal solutions in drug delivery wherein stable dispersions are required. The zeta potential of 30 weeks stored colloidal solution of bio-stabilized AuNP was −30 mV, which suggests the fair redespersibility of the particles which is shown in Fig. 11 [33]. The increase in the particle size of the AuNP as mentioned in the figure may be because of the agglomeration of the colloids or the increased organic capping on the surface of the AuNP. The entire exercise infers that AuNP synthesized and stored for 30 weeks at room temperature were much more stable than the nanoparticles synthesized from the other biological routes. Bio-functionalization, i.e., the nature of capping conferring the stability of the AuNP obtained by this method, is quite important, as this method produces extremely stable metallic nanoparticles.

Conclusion

Rapid synthesis and excellent reproducibility of gold nanoparticles through this method has the time-related advantage in comparison with microbial synthesis and avoids all lengthy, laborious processes and also hygienic complications associated with them. Using the clean-green chemistry involved in this way, we can think of the industrial scaling of nanoparticles. This field of gold nanoparticle biosynthesis is leading to new avenues in material science, chemistry, nanobiotechnology and biotechnology. In future, it would be significant to understand the clear mechanism of biosynthesis and to technologically engineer the nanoparticles in order to achieve better control over size, shape, and absolute monodispersivity.

Acknowledgments Financial supports from DST (grant no.SR/S1/PC-10/2005), UGC (D.O. no.F.14-4/2001 (Innov.Policy/ASIST)), and BRNS, DAE (no. 2009/34/BRNS) are acknowledged. We thank Prof. G. U. Kulkarni for fruitful guidance and Selvi Rajan, JNCASR Bangalore for FESEM measurements. We are grateful to Prof. Manohar Badiger (NCL, Pune) for zeta potential measurements. Raghunandan Deshpande thanks Dr. Appala Raju, Principal of HKES College of pharmacy, Gulbarga for encouraging the research program.

References

1. Chen C, Sandra CM, Oyelere AK. Gold nanoparticles: From nanomedicine to nanosensing. Nanotechnology, Science and Applications. 2008;1:45.
2. Salata OV. Application of nanoparticles in biology and medicine. J Nanobiotechnology. 2004;2:3.
3. El-Sayed M. Small is different: shape-, size-, and composition-dependent properties of some colloidal semiconductor nanocrystals. Acc Chem Res. 2004;37(5):326.
4. Kim F, Connor S, Song H, Kuykendall T, Yang P. Platonic gold nanocrystals. Angew Chem. 2004;116:3759.
5. Yakimovich NO, Ezhevskii AA, Guseinov DV, Smirnova LA, Gracheva TA, Klychkov KS. Antioxidant properties of gold nanoparticles studied by ESR spectroscopy. Russ Chem Bull. 2008;57(3):520.
6. Jing-Liang L, Wang L, Xiang-Yang L, Zhang Z, Hong-Chen G, Wei-Min L, et al. In vitro cancer cell imaging and therapy using transferrin-conjugated gold nanoparticles. Cancer Lett. 2009;27(2):319.
7. Sperling RA, PR Gil PR, Zhang F, Zanella M, Parak WJ. Biological applications of gold nanoparticle. Chem Soc Rev. 2008;37:1896.
8. Greenfield AS. Biotechnology, the brain and the future. Trends Biotech. 2005;23(1):34.
9. Kevin B. Shape Matters for Nanoparticles; Technology published by MIT review; 2008.
10. Gobin MA, Lee MH, Naomi JH, William DJ, Rebekah AD, Jennifer LW. Near- infrared resonant nanoshells for combined optical imaging and photothermal cancer therapy. Nano Lett. 2007;7(7):1929.
11. Bertussi B, Natoli JY, Commandre M, Rullier JL, Bonneau F, Combis P, et al. Photothermal investigation of the laser-induced modification of a single gold nano-particle in a silica film. Opt Commun. 2005;254(4):299.

12. Kannan R, Rahing V, Cutler CS, Pandrapragada RK, Katti KK, Kattumuri VJ, et al. Nanocompatible chemistry toward fabrication of target-specific gold nanoparticles. J Am Chem Soc. 2006;128:11342.
13. Rinaldo P, Matteo G, Maila S. Nanosystems, in inorganic and bio-inorganic chemistry. In: Bertini I, editor. Encyclopedia of Life Support Systems (EOLSS), Developed under the Auspices of the UNESCO. Oxford, UK: Eolss Publishers 2006.
14. Jianqiang H, Zhouping H, Jinghong L. Gold nanoparticles with special shapes: controlled synthesis, surface-enhanced Raman scattering, and the application in biodetection. Sensors. 2007;7:3299.
15. He L, Musick MD, Nicewarner SR, Salinas FG, Benkovic SJ, Natan MJ, et al. Colloidal Au-enhanced surface plasmon resonance for ultrasensitive detection of DNA hybridization. J Am Chem Soc. 2000;122:9071.
16. Maxwell DJ, Taylor JR, Nie SM. Self-assembled nanoparticle probes for recognition and detection of biomolecules. J Am Chem Soc. 2002;124:9606.
17. Haynes CA, Nordle W. Globular proteins at solid/liquid interfaces. Coll Surf B: Biointerfaces. 1994;2:517.
18. Ahmad A, Mukherjee P, Senapati S, Mandal D, Khan MI, Kumar R, et al. Extracellular biosynthesis of silver nanoparticles using the fungus *Fusarium oxysporum*. Coll Surf B: Biointerfaces. 2008;28:313.
19. Basavaraja S, Balaji SD, Lagashetty A, Rajasab AH, Venkataraman A. Extracellular biosynthesis of silver nanoparticles using the fungus *Fusarium semitectum*. Mater Res Bull. 2008;43:1164.
20. Balaji DS, Basavaraja S, Raghunandan D, DB Mahesh D, Venkataraman A. Biosynthesis and stabilization of Au and Au–Ag alloy nanoparticles by fungus, *Fusarium semitectum*. Sci Technol Adv Mater. 2008;9:035012.
21. Balaji DS, Basavaraja S, Raghunandan D, Mahesh B, Prabhakar BK, Venkataraman A. Extracellular biosynthesis of functionalized silver nanoparticles by strains of *Cladosporium cladosporioides* fungus. Coll Surf B: Biointerfaces. 2009;68(1):88.
22. Gardea-Torresdey LJ, Gomez E, Peralta-Videa RJ, Parsons JG, Troiani H, Jose-Yacaman M. Alfalfa sprouts: a natural source for the synthesis of silver nanoparticles. Langmuir. 2003;19(4):1357.
23. Shiv Shankar S, Rai A, Ahmad A, Sastry M. Rapid synthesis of Au, Ag, and bimetallic Au core–Ag shell nanoparticles using Neem (*Azadirachta indica*) leaf broth. J Colloid Interface Sci. 2004;275(2):496.
24. Kawakami Y, Nakamura T, Hosokawa T, Suzuki-Yamamoto T, Yamashita H, Kimoto M, et al. Antiproliferative activity of guava leaf extract via inhibition of prostaglandin endoperoxide H synthase isoforms. Prostaglandins, Leukot Essent Fat Acids. 2009;80(5-6):239.
25. Manosroi J, Dhumtanom P, Manosroi A. Antiproliferative activity of essential oil extracted from Thai medicinal plants on KB and P388 cell lines. Cancer Lett. 2006;235:114.
26. Chen KC, Hsieh CL, Peng CC, Hsieh-Li HM, Chiang HS, Huang KD, et al. Brain derived metastatic prostate cancer DU-145 cells are effectively inhibited in vitro by guava (*Psidium gujava* L.) leaf extracts. 58(1). Nutr Cancer. 2007;58:93.
27. Gutierrez RM, Mitchell S, Solaris RV. *Psidium guajava*: A review of its traditional uses, phytochemistry and pharmacology. J. Ethnopharmacol. 2008;117(1):1.
28. Choi SY, Hwang JH, Park SY, Jin YJ, Ko HC, Moon SW, et al. Fermented guava leaf extract inhibits LPS-induced COX-2 and iNOS expression in mouse macrophage cells by inhibition of transcription factor NF-kB. Phytother Res. 2008;22:1030.
29. Mulvaney P. Surface plasmon spectroscopy of nanosized metal particles. Langmuir. 1996;12:788.
30. Robert BB, David JB, Toca-Herrera LJ, Blake AW, Smith DA, Radford SE, et al. Force mode atomic force microscopy as a tool for protein folding studies. Anal Chim Acta. 2003;479(1):87.
31. Suganya T, Ikegami F, Okonogi S. Antioxidant active principles isolated from *Psidium guajava* grown in Thailand. Sci Pharm. 2007;75:179.
32. Begum S, Hassan SI, Ali SN, Siddiqui BS. Chemical constituents from the leaves of *Psidium guajava*. Nat Prod Res. 2004;18 (2):135.
33. Zeta potential of colloids in water and waste water, ASTM standard D 4187-82, American society for testing and materials, 1985.